

A non-conforming least-squares finite element method for the velocity-vorticity-pressure Stokes equations

Pavel Bochev^{1,*}, James Lai² and Luke Olson²

¹ *Numerical Analysis and Applications Department, Sandia National Laboratories, Mail Stop 1320, Albuquerque, New Mexico, 87185-1320*

² *Department of Computer Science, University of Illinois at Urbana-Champaign, Urbana, IL 61801.*

SUMMARY

In this paper, we focus on the formulation of least-squares finite element methods (LSFEM) for incompressible fluid flows with improved mass conservation. Specifically, we formulate a new locally conservative LSFEM for the velocity-vorticity-pressure Stokes system, which uses a piecewise divergence-free basis for the velocity and standard C^0 elements for the vorticity and the pressure. The new method, which we term dV-VP improves upon the discontinuous stream function formulation [6] in several aspects. The use of a velocity basis, instead of a stream function, simplifies the imposition and implementation of the velocity boundary condition, and eliminates second order terms from the least-squares functional. Moreover, the size of the resulting discrete problem is reduced since the piecewise solenoidal velocity element is approximately one half of the dimension of a stream function element of equal accuracy. We show that performance of the dV-VP LSFEM can be further improved by additional interelement terms motivated by the discontinuous stream function LSFEM [6]. Computational studies demonstrate that the new formulation achieves optimal convergence rates and yields high conservation of mass. We also propose a simple diagonal preconditioner for the dV-VP formulation, which significantly reduces the condition number of the LSFEM problem. Copyright © 2011 John Wiley & Sons, Ltd.

Received ...

KEY WORDS: Least-squares finite element methods, discontinuous elements, Stokes equations, piecewise divergence free velocity, stream function, vorticity, pressure, mass conservation.

1. INTRODUCTION

Least-squares finite element methods (LSFEMs) for partial differential equations (PDEs) cast PDEs into unconstrained minimization problems for artificial least-squares “energy” functionals. Summation of equation residuals measured in suitable Sobolev space norms defines the least-squares functional.

Least-squares methods offer valuable computational and theoretical properties. For example, norm-equivalent least-squares functionals give rise to symmetric, strongly coercive variational

*Correspondence to: Sandia National Laboratories, Mail Stop 1320, Albuquerque, New Mexico, 87185-1320. E-mail: pbboche@sandia.gov

Contract/grant sponsor: Sandia National Laboratories is a multi-program laboratory operated by Sandia Corporation, a wholly owned subsidiary of Lockheed Martin Corporation, for the U.S. Department of Energy’s National Nuclear Security Administration under contract DE-AC04-94AL85000.

Contract/grant sponsor: This work was partially supported by the NSF; contract/grant number: DMS 07-46676.

problems, and a stable and accurate finite element discretization does not require restrictive inf-sup conditions between the finite element spaces. As a result, the associated algebraic systems of equations are symmetric and positive definite and are often amenable to efficient iterative methods such as preconditioned conjugate gradients.

However, one drawback in conventional C^0 LSFEMs for incompressible fluid flows, is the lack of control of mass conservation, which in some cases leads to highly inaccurate results [10, 25]. The published remedies include the restricted least-squares method [10], high-order (spectral and hp) least-squares methods [24, 25], and mimetic least-squares methods [4, Section 7.7], [5]. While these approaches succeed in improving mass conservation, they remain more complex to implement than standard mixed Galerkin methods and often require non-standard boundary conditions and/or structured grids, thus conceding several of the advantages of least-squares principles.

This paper continues the effort of [6] to develop least-squares methods, which improve mass conservation, while remaining straightforward to implement and solve using publicly available libraries such as the Trilinos [17] packages Intrepid [7] and ML [15]. The discontinuous stream function, continuous vorticity and pressure method (dS-VP) [6] uses a discontinuous stream function to obtain a locally divergence-free finite element solution of the Stokes equations. The method achieves nearly perfect conservation of mass on a series of challenging test problems, yet requires the use of an additional stream function.

In this paper, we present a new discontinuous velocity, continuous vorticity-pressure (dV-VP) LSFEM for the Stokes equations. Our goal is to develop alternatives that improve upon the dS-VP formulation by directly employing a piecewise solenoidal basis [1] for the velocity. As a result, we eliminate second order terms from the least-squares functional, simplify implementation of the velocity boundary condition, and reduce the minimal admissible polynomial order from 3, in the dS-VP method, to 2, which is equal to that of the stable Taylor-Hood element pair [16]. Because the dimension of the piecewise solenoidal velocity element is approximately one half of the dimension of a stream function element with comparable accuracy, the size of the resulting algebraic problem is reduced.

A discontinuous velocity least-squares functional typically involves only the standard jump terms in the velocity field across element interfaces. We show that mass conservation is stronger for certain problems when the dV-VP least-squares functional is augmented with additional jump terms, as motivated by the dS-VP method. Computational studies support these additional terms in the dV-VP LSFEM by showing optimal convergence rates and by highlighting the mass conservation properties in the approximation. Introducing discontinuous terms also affects the conditioning of the problem. Yet, we demonstrate that a simple diagonal preconditioner is effective for the dV-VP algebraic problem.

In Section 2 we summarize notation, the governing equations, various least-squares formulations relevant to this paper, and introduce test problems for the computational studies. In Section 3, we present the new dV-VP LSFEM by introducing a series of intermediate functionals, as outlined in the following:

$$J_{(h)}^S \xrightarrow{\psi \text{ to } \mathbf{u}} J_{(h)}^V \xrightarrow{\text{modify jump}} \widehat{J}_{(h)}^V \xrightarrow{\text{implicit } \psi} \widetilde{J}_{(h)}^V, \quad (1)$$

where $J_{(h)}^S$ is the dS-VP functional from [6]. We then introduce $J_{(h)}^V$, wherein the stream function is replaced by a divergence-free velocity basis, followed by $\widehat{J}_{(h)}^V$ in which jump terms are used to accommodate for the difference in scaling of the divergence-free velocity basis, and finally we use $\widetilde{J}_{(h)}^V$ to enforce global continuity of an implicit stream function. We also define a diagonal preconditioner for the discrete problems and in Section 4 we focus on computational studies of the dV-VP formulation, which includes convergence rates, conservation of mass, preconditioning, and impact of the divergence-free basis choice on the properties of the LSFEMs. We summarize our conclusions in Section 5.

2. QUOTATION OF RESULTS

2.1. Notation

For clarity we restrict our attention to two space dimensions and bounded, simply connected regions $\Omega \subset \mathbb{R}^2$ with a Lipschitz-continuous boundary $\Gamma = \partial\Omega$. We adhere to the standard notation, $H^k(\Omega)$, for a Sobolev space of order k with norm and inner product given by $\|\cdot\|_k$ and $(\cdot, \cdot)_k$, respectively. When $k = 0$ we write $L^2(\Omega)$, (\cdot, \cdot) , and $\|\cdot\|_0$. The subspace of $H^1(\Omega)$ functions with vanishing trace on $\partial\Omega$ is $H_0^1(\Omega)$ and $L_0^2(\Omega)$ is the subspace of L^2 -fields with zero mean. We denote by $H^{-1}(\Omega)$ the dual of $H_0^1(\Omega)$ with norm

$$\|u\|_{-1} = \sup_{v \in H_0^1(\Omega)} \frac{(u, v)}{\|v\|_1}. \quad (2)$$

Vectors and vector valued function spaces are denoted by bold face symbols — e.g., $\mathbf{u} = (u_1, u_2)$ and $\mathbf{H}^1(\Omega)$ — with the Euclidean norm on \mathbb{R}^n given by $|\cdot|$. In two-dimensions the curl is defined for scalar and vector functions by

$$\nabla \times \omega = \begin{bmatrix} \omega_y \\ -\omega_x \end{bmatrix} \quad \text{and} \quad \nabla \times \mathbf{u} = (u_2)_x - (u_1)_y, \quad (3)$$

respectively.

We consider a conforming finite element partition $\mathcal{K}_h = \{\kappa\}$ of the domain Ω , where, in two dimensions, κ is either a quadrilateral or a triangle. Two neighboring elements share an edge, ε , and we denote the set of all edges in the mesh \mathcal{K}_h as \mathcal{E}_h and the set of all interior edges as $\mathcal{E}_{h,0}$.

The discontinuous methods in this paper use standard jump operators on element interfaces. Let κ^+ and κ^- be two adjacent elements that share edge ε , and let ψ^+ and ψ^- be the restrictions of a piecewise smooth function ψ on these elements. The jump of ψ across the interface is the difference of its states along ε :

$$[\psi] := (\psi^+ - \psi^-)|_\varepsilon. \quad (4)$$

Furthermore, component-wise application of the scalar jump operator (4) defines a jump operator for a piecewise smooth vector field \mathbf{u} :

$$[\mathbf{u}] := ([u_1], [u_2]). \quad (5)$$

2.2. Standard C^0 finite element spaces

We assume that \mathcal{K}_h is quasi-uniform [12], where the elements in \mathcal{K}_h are images of a standard (reference) element $\widehat{\kappa}$ under a smooth map $F_\kappa : \widehat{\kappa} \mapsto \kappa$, where $J_\kappa = \nabla F_\kappa$. The approximating space on each element is defined by suitable transformation of the reference space $R_r(\widehat{\kappa})$. In the case of a simplex $\widehat{\kappa}$, $R_r(\widehat{\kappa}) = P_r(\widehat{\kappa})$ is the space of all polynomials of degree r , whereas in the case of a square $\widehat{\kappa}$, $R_r(\widehat{\kappa}) = Q_r(\widehat{\kappa})$ is the space of all polynomials whose degree in each coordinate direction does not exceed r .

The standard C^0 finite element spaces of degree $r > 0$ on quadrilateral and triangular grids are

$$R_r(\Omega) = \{v_h \in H^1(\Omega) \mid v_h|_\kappa = \widehat{v}_h \circ F_\kappa^{-1}; \widehat{v}_h \in R_r(\widehat{\kappa})\}. \quad (6)$$

Here, $[R_r](\Omega)$ is the discontinuous version of these spaces. The coefficients of a finite element function v_h relative to a basis are a vector $\vec{v} \in \mathbb{R}^n$.

Next, we recall several key properties of standard finite elements (6) on quasi-uniform grids.

Approximation. For every $v \in H^{r+1}(\Omega)$ there exists $I(v) \in R_r(\Omega)$ such that

$$\|v - I(v)\|_0 + h\|v - I(v)\|_1 \leq Ch^{r+1}\|v\|_{r+1}, \quad (7)$$

where C is independent of h .

Inverse inequalities. There exists positive constants C_1 and C_2 , independent of h , such that for every element $\kappa \in \mathcal{K}_h$

$$C_1 h^2 |\vec{v}|^2 \leq \|v_h\|_{0,\kappa} \leq C_2 h^2 |\vec{v}|^2. \quad (8)$$

Additionally, finite element functions satisfy the inverse inequalities

$$\|v_h\|_{1,\kappa} \leq Ch^{-1}\|v_h\|_{0,\kappa} \quad \text{and} \quad \|v_h\|_{1/2,e} \leq Ch^{-1/2}\|v_h\|_{0,e} \quad (9)$$

These inequalities hold whenever the mesh is quasi-uniform and the finite element spaces are defined by transformation of a reference space as in (6) [14, Lemma 9.7, p.386; Lemma 1.138, p.75]. In finite element methods that involve mesh-dependent terms, such as weighted least-squares methods and discontinuous finite element methods, validity of inverse inequalities is required to maintain the proper scaling of these mesh dependent terms.

2.3. Piecewise divergence-free velocity element

In this paper we use a piecewise solenoidal velocity element \mathbf{V}_r , with $r \geq 1$, as proposed in [1]. The dimension of \mathbf{V}_r depends only on the polynomial degree r and not on the shape of the reference element $\hat{\kappa}$. For example the linear piecewise solenoidal space in two dimensions is

$$\mathbf{V}_1(\hat{\kappa}) = \left\{ \begin{pmatrix} 1 \\ 0 \end{pmatrix}, \begin{pmatrix} 0 \\ 1 \end{pmatrix}, \begin{pmatrix} y \\ 0 \end{pmatrix}, \begin{pmatrix} 0 \\ x \end{pmatrix}, \begin{pmatrix} x \\ -y \end{pmatrix} \right\}, \quad (10)$$

while the quadratic space is

$$\mathbf{V}_2(\hat{\kappa}) = \mathbf{V}_1(\hat{\kappa}) \cup \left\{ \begin{pmatrix} y^2 \\ 0 \end{pmatrix}, \begin{pmatrix} 0 \\ x^2 \end{pmatrix}, \begin{pmatrix} x^2 \\ -2xy \end{pmatrix}, \begin{pmatrix} -2xy \\ y^2 \end{pmatrix} \right\}. \quad (11)$$

In d -dimensions, we arrive at

$$\dim \mathbf{V}_r(\hat{\kappa}) = \frac{d(d+r)! - (d+r-1)!r}{d!r!}.$$

We define the full velocity space $\mathbf{V}_r(\Omega)$ by translation and scaling of the reference element space

$$\mathbf{V}_r(\Omega) = \{v_h \in \mathbf{L}^2(\Omega) \mid v_h(\mathbf{x})|_{\kappa} = \hat{v}_h(\mathbf{x} - \mathbf{b}_{\kappa})/J_{\kappa}^{(\deg \hat{v})/2}; \hat{v}_h \in \mathbf{V}_r(\hat{\kappa})\}, \quad (12)$$

where $\deg \hat{v}$ is the polynomial degree of basis function \hat{v}_h and \mathbf{b}_{κ} is the barycenter of element κ .

Remark 1

Inequalities such as (8) and (9) motivate the mesh-dependent weights in weighted least-squares functionals. However, the varying polynomial degrees of the basis functions in $\mathbf{V}_r(\hat{\kappa})$ prevent (8) and (9) from holding. By using translation and mesh-dependent scaling proportional to the polynomial degree of each basis function we are able to define piecewise solenoidal bases for $\mathbf{V}_r(\Omega)$ that satisfy inverse inequalities. We note that this is similar to the piecewise divergence free basis defined in [13], but uses a different scaling for which the mass matrix is not spectrally equivalent to a scaled identity.

The velocity space (12) is completely discontinuous and is not H^1 -conforming, yet $\mathbf{V}_r(\Omega)$ exhibits an optimal approximation property [1, Theorem 4.3]: for every $\mathbf{v} \in \mathbf{H}^{r+1}(\kappa)$ there exists $I(\mathbf{v}) \in \mathbf{V}_r(\kappa)$ such that

$$\|\mathbf{v} - I\mathbf{v}\|_{j,\kappa} \leq Ch^{r+1-j}|\mathbf{v}|_{r+1,\kappa}; \quad j = 0, \dots, r. \quad (13)$$

For examples of Discontinuous Galerkin methods, which use \mathbf{V}_r elements we refer to [13, 22] and the references therein. The paper [1] also compares \mathbf{V}_r elements with other nonconforming spaces such as Crouzeix-Raviart elements [23].

2.4. The velocity-vorticity-pressure Stokes system

It is common to define least-squares finite element methods using the first-order system form of the governing PDEs. The Stokes equations admit several such forms [4, Section 7.1]. Here, we choose

to work with the velocity-vorticity-pressure (VVP) first-order system

$$\nabla \times \omega + \nabla p = \mathbf{f} \quad \text{on } \Omega \quad (14a)$$

$$\omega - \nabla \times \mathbf{u} = 0 \quad \text{on } \Omega \quad (14b)$$

$$\nabla \cdot \mathbf{u} = 0 \quad \text{on } \Omega. \quad (14c)$$

The system (14) is augmented with the velocity boundary condition

$$\mathbf{u} = 0 \quad \text{on } \partial\Omega \quad (15)$$

and the zero mean pressure constraint

$$\int_{\Omega} p \, d\Omega = 0. \quad (16)$$

Each component of (14) plays a role in the solution: (14a) governs conservation of momentum, (14b) defines the vorticity, and (14c) is the continuity equation, which governs conservation of mass. The VVP Stokes equations have been studied extensively in the context of least-squares finite element methods [3, 8, 11, 18, 19, 20, 21] and the mathematical and computational properties of conforming LSFEMs for (14) are well-understood.

2.5. Standard C^0 least-squares methods for the velocity-vorticity-pressure Stokes system

We next review two conforming LSFEMs for (14), which motivate the new methods proposed in this paper. In both cases the starting point is the least-squares functional

$$J_{-1}(\mathbf{u}, \omega, p; \mathbf{f}) = \|\nabla \times \omega + \nabla p - \mathbf{f}\|_{-1}^2 + \|\nabla \times \mathbf{u} - \omega\|_0^2 + \|\nabla \cdot \mathbf{u}\|_0^2, \quad (17)$$

which is norm equivalent on $X = \mathbf{H}_0^1(\Omega) \times L^2(\Omega) \times L_0^2(\Omega)$ — see [2]. Norm-equivalence leads to a well-posed formulation of the least-squares, unconstrained minimization problem: find $(\mathbf{u}, \omega, p) \in X$ such that

$$J_{-1}(\mathbf{u}, \omega, p; \mathbf{f}) \leq J_{-1}(\mathbf{v}, \xi, q; \mathbf{f}) \quad \forall (\mathbf{v}, \xi, q) \in X. \quad (18)$$

Here, the unique minimizer coincides with the solution of the VVP Stokes system (14).

A specific LSFEM emerges by choosing an approximation to the $\|\cdot\|_{-1}$ term in (17). One method is the *weighted* LSFEM [3]

$$J_h(\mathbf{u}_h, \omega_h, p_h; \mathbf{f}_h) = h^2 \|\nabla \times \omega_h + \nabla p_h - \mathbf{f}_h\|_0^2 + \|\nabla \times \mathbf{u}_h - \omega_h\|_0^2 + \|\nabla \cdot \mathbf{u}_h\|_0^2 \quad (19)$$

in which the negative norm is approximated by the weighted L^2 norm $h\|\cdot\|_0$, while another method is the *discrete negative norm* LSFEM

$$J_{-h}(\mathbf{u}_h, \omega_h, p_h; \mathbf{f}_h) = \|\nabla \times \omega_h + \nabla p_h - \mathbf{f}_h\|_{-h}^2 + \|\nabla \times \mathbf{u}_h - \omega_h\|_0^2 + \|\nabla \cdot \mathbf{u}_h\|_0^2 \quad (20)$$

in which the negative norm is approximated by $\|\cdot\|_{-h} = h^2\|\cdot\|_0^2 + \|(\mathcal{L}_h)^{1/2} \cdot\|_0^2$, where \mathcal{L}_h is a spectrally equivalent preconditioner for the Laplace operator [9]. For brevity we denote both norms and the associated least-squares functionals by the common symbols $\|\cdot\|_{(h)}$ and $J_{(h)}$, respectively.

A well-posed discrete least-squares principle for (19)–(20) is the following: find $(\mathbf{u}_h, \omega_h, p_h) \in X_h^r$ such that

$$J_{(h)}(\mathbf{u}_h, \omega_h, p_h; \mathbf{f}_h) \leq J_{(h)}(\mathbf{v}_h, \xi_h, q_h; \mathbf{f}_h) \quad \forall (\mathbf{v}_h, \xi_h, q_h) \in X_h^r, \quad (21)$$

where

$$X_h^r = \mathbf{R}_r(\Omega) \cap \mathbf{H}_0^1(\Omega) \times R_{r-1}(\Omega) \times R_{r-1}(\Omega) \cap L_0^2(\Omega) \quad (22)$$

with $r \geq 1$ for the discrete negative norm LSFEM, and $r > 1$ for the weighted[†] LSFEM.

Both least-squares methods converge optimally for all sufficiently regular solutions of (14), as summarized in the following, while additional theoretical and computational properties of (20) and (19) are found in [4].

[†]The *minimal approximation condition* $r > 1$ is required for optimal convergence rates. Using $R_1(\Omega)$ elements for all variables in (22), for example, reduces the accuracy of the least-squares solution; see [3].

Theorem 1 (Optimal Convergence [4, Theorem 7.14, p.262])

Let $(\mathbf{u}_h, \omega_h, p_h) \in X_h^r$ with $r > 1$ be a solution to (19) and assume that $(\mathbf{u}, \omega, p) \in \mathbf{H}^{r+2}(\Omega) \times H^{r+1}(\Omega) \times H^{r+1}(\Omega)$ is the exact solution of the VVP Stokes system (14). There exists a constant $C > 0$ such that

$$\|\mathbf{u} - \mathbf{u}_h\|_1^2 + \|\omega - \omega_h\|_0 + \|p - p_h\|_0 \leq Ch^{r+1} (\|\mathbf{u}\|_{r+2} + \|\omega\|_{r+1} + \|p\|_{r+1}) \quad (23a)$$

and

$$\|\omega - \omega_h\|_1 + \|p - p_h\|_1 \leq Ch^r (\|\mathbf{u}\|_{r+2} + \|\omega\|_{r+1} + \|p\|_{r+1}). \quad (23b)$$

The error estimate (23) holds for (20) provided $r \geq 1$.

Remark 2

The error estimates in Theorem 1 hold for the equal order spaces

$$X_h^{(r)} = \mathbf{R}_r(\Omega) \cap \mathbf{H}_0^1(\Omega) \times R_r(\Omega) \times R_r(\Omega) \cap L_0^2(\Omega). \quad (24)$$

Such spaces have more degrees of freedom but their uniform data structure simplifies implementation of least-squares methods.

2.6. Discontinuous stream function, vorticity-pressure least-squares method (dS-VP)

The approach presented in [6] is to consider discontinuous velocity fields in (19)–(20) and then to represent the velocity on each element by a curl of a discontinuous stream function. The resulting *discontinuous stream function, continuous vorticity-pressure* (dS-VP) version of $J_{(h)}$ is given by

$$\begin{aligned} J_{(h)}^S(\psi_h, \omega_h, p_h; \mathbf{f}_h) &= \|\nabla \times \omega_h + \nabla p_h - \mathbf{f}_h\|_{(h)}^2 + \sum_{k \in K(\Omega)} \|\nabla \times \nabla \times \psi_h - \omega_h\|_{0,k}^2 \\ &+ \sum_{e \in E(\Omega)} h^{-1} \|\nabla \times \psi_h\|_{0,e}^2 + h^{-3} \|\psi_h\|_{0,e}^2 + \sum_{e \in E(\Gamma)} h^{-1} \|(\nabla \times \psi_h) \times \mathbf{n}_i\|_{0,e}^2 \end{aligned} \quad (25)$$

Computational results in [6] confirm that the dS-VP formulation attains high mass conservation. Our key objective is to achieve similar mass conservation while avoiding some practical inconveniences of stream functions. As an example, for the velocity boundary condition, a Dirichlet boundary condition for the stream function requires the identity $\mathbf{u} \cdot \mathbf{n} = (\nabla \times \psi) \cdot \mathbf{n}$, while still requiring enforcement of the tangential velocity component. For the weighted LSFEM (19), the minimal approximation condition $r > 1$ implies that the stream function requires approximation by at least cubic or bi-cubic elements. These elements have nearly twice the degrees of freedom of the piecewise solenoidal element (10) and require more accurate quadrature than quadratic elements. Additionally, the second order terms in (25) also result in higher condition numbers, leading to increased computational demands on the algebraic solver.

2.7. Test problems

To assess mass conservation properties of various LSFEMs we use the following test problems: the backward-facing step flow (Figure 1), a channel flow past a cylinder (Figure 2), a split channel flow (Figure 3), and a restricted channel flow (Figure 4). In order to keep the mass loss computations comparable between test domains, each mesh is well refined and generated by using an average element size of $h \approx 0.03 - 0.04$.

Test Problem 1 (Backward-facing step)

For the backward-facing step the computational domain Ω is the rectangle $[0, 10] \times [0, 1]$ with a reentrant corner at $(2, 0.5)$. The velocity boundary conditions on the inflow ($x = 0$), outflow ($x = 10$), and horizontal walls are given by

$$\mathbf{u}_{in} = \begin{bmatrix} 8(y - 0.5)(1 - y) \\ 0 \end{bmatrix}, \mathbf{u}_{out} = \begin{bmatrix} y(1 - y) \\ 0 \end{bmatrix}, \text{ and } \mathbf{u}_{wall} = \mathbf{0}, \quad (26)$$

respectively. For this problem we use \mathcal{K}_h comprised of 6442 triangles.

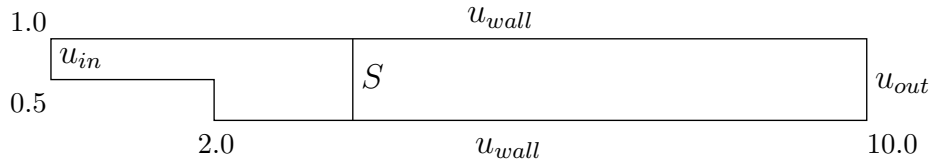


Figure 1. Geometry of Test Problem 1: backward-facing step.

Test Problem 2 (Cylinder)

The computational domain Ω for the cylinder problem is the rectangle $[-1, 3] \times [-1, 1]$ with a disk-shaped obstacle of radius $r > 0$ centered at $(0, 0)$. The difficulty of this test increases as the radius reduces the size of the gap above and below the disk. In our example, we use $r = 0.9$. The velocity boundary conditions on the inflow ($x = -1$), outflow ($x = 3$), top ($y = 1$), and bottom ($y = -1$) walls are given by

$$\mathbf{u}_{in} = \mathbf{u}_{out} = \mathbf{u}_{wall} = \begin{bmatrix} (1-y)(1+y) \\ 0 \end{bmatrix}, \quad (27)$$

while on the surface of the cylinder we impose $\mathbf{u}_{cyl} = \mathbf{0}$. We solve this test problem on \mathcal{K}_h with 6011 triangles.

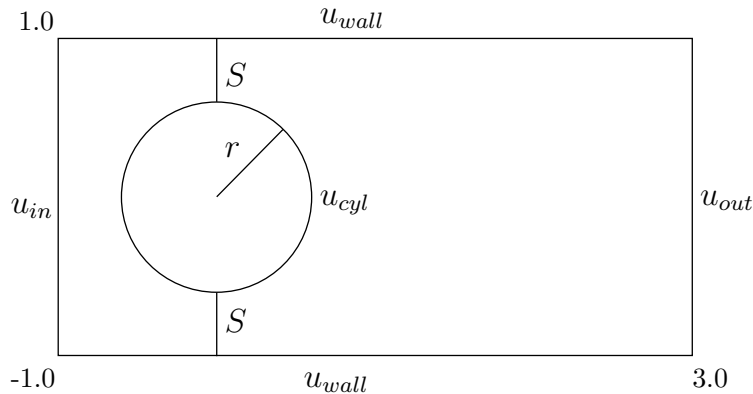


Figure 2. Geometry of Test Problem 2: flow past a cylinder.

Test Problem 3 (Split channel)

In this example, we model channel flow split into two separate channels and then finally combining back into a single channel. The computational domain begins with a height of 1 and splits off into two channels of height 0.5. For the boundary conditions, we set

$$\mathbf{u}_{in} = \mathbf{u}_{out} = \begin{bmatrix} (0.5-y)(0.5+y) \\ 0 \end{bmatrix}, \text{ and } \mathbf{u}_{wall} = \mathbf{0}. \quad (28)$$

This test problem is solved on \mathcal{K}_h with 6694 triangles.

Test Problem 4 (Restricted channel)

For the restricted channel domain, we have a channel flow that is pinched in on the top and bottom sides. The domain is the rectangular domain $[-2, 2] \times [-1, 1]$. The channel is pinched in at $x = 0$ using two semi-cylindrical cut outs of radius r . Similar to the cylinder flow domain, the larger the radius, the more narrow the opening of the channel and hence increasing the difficulty of the problem. In our examples, we use $r = 0.9$. The boundary conditions are set as in (27) and the domain is meshed using 4124 triangles.

In each of the test problems the boundary conditions are compatible with $\nabla \cdot \mathbf{u} = 0$. To assess mass conservation we follow the procedure from [6] and measure the total mass flow across a

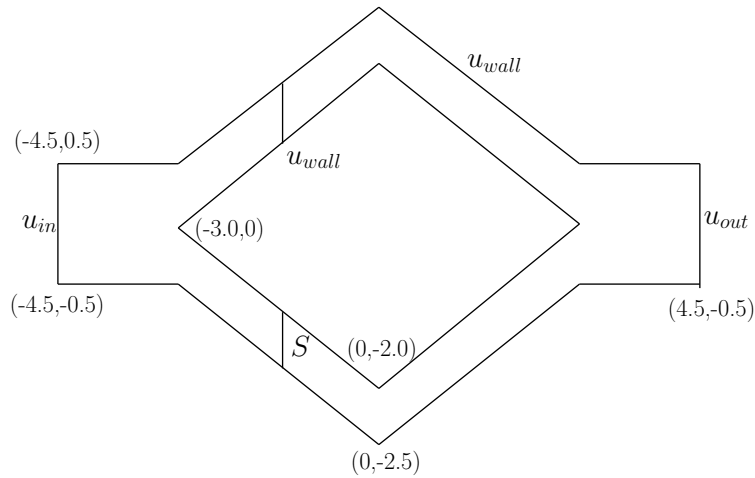


Figure 3. Geometry of Test Problem 3: split channel.

sequence of vertical surfaces connecting the top and the bottom sides of the computational domain. The lines denoted by S in Figures 1-4 show examples of such surfaces.

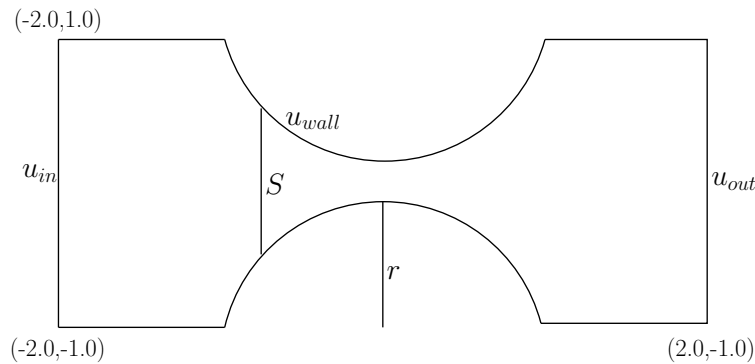


Figure 4. Geometry of Test Problem 4: restricted channel.

Since $\mathbf{u} = \mathbf{0}$ on all parts of $\partial\Omega$ except Γ_{in} and Γ_{out} in each test problem, the Divergence Theorem implies

$$\int_{\Gamma_{in}} \mathbf{u} \cdot \mathbf{n}_{in} \, dl = \int_S \mathbf{u} \cdot \mathbf{n}_S \, dl, \quad (29)$$

for any S connecting the top and bottom walls of the domain. Therefore, mass conservation is quantified by the percent mass loss across the surface S , defined as follows:

$$\%m_{loss} = \frac{\int_{\Gamma_{in}} \mathbf{u} \cdot \mathbf{n}_{in} \, dl - \int_S \mathbf{u} \cdot \mathbf{n}_S \, dl}{\int_{\Gamma_{in}} \mathbf{u} \cdot \mathbf{n}_{in} \, dl} \times 100. \quad (30)$$

3. DISCONTINUOUS VELOCITY VORTICITY-PRESSURE LEAST-SQUARES METHOD

For clarity we develop the new dV-VP formulation in three stages. The first stage reprises the approach of [6] to relax the C^0 continuity for the velocity space only. Therefore, we change the

approximating space from (22) to

$$\tilde{X}_h^r = [\mathbf{R}_r](\Omega) \times R_{r-1}(\Omega) \times R_{r-1}(\Omega) \cap L_0^2(\Omega) \quad (31)$$

or its equal-order counterpart

$$\tilde{X}_h^{(r)} = [\mathbf{R}_r](\Omega) \times R_r(\Omega) \times R_r(\Omega) \cap L_0^2(\Omega) \quad (32)$$

and modify $J_{(h)}$ in (19) and (20) to allow discontinuous velocity fields:

$$\begin{aligned} J_{(h)}^V(\mathbf{u}_h, \omega_h, p_h; \mathbf{f}_h) &= \|\nabla \times \omega_h + \nabla p_h - \mathbf{f}_h\|_{(h)}^2 \\ &+ \sum_{\kappa \in \mathcal{K}_h(\Omega)} \left(\|\nabla \times \mathbf{u}_h - \omega_h\|_{0,\kappa}^2 + \|\nabla \cdot \mathbf{u}_h\|_{0,\kappa}^2 \right) + \sum_{\varepsilon \in \mathcal{E}_{h,0}} h^{-1} \|[\mathbf{u}_h]\|_{0,\varepsilon}^2. \end{aligned} \quad (33)$$

Numerical results in [6] show that (33) conserves mass poorly even if tangential and normal jumps of the velocity are weighted differently. To improve mass conservation in [6] we used a discontinuous stream function and the associated dS-VP formulation (25). In this paper we, adopt a different approach and approximate the velocity directly using the piecewise solenoidal discontinuous space $\mathbf{V}_r(\Omega)$ as defined in Section 2.3. Thus, at the second stage we replace the discrete minimization spaces (31) and (32) by

$$\overline{X}_h^r = \mathbf{V}_r(\Omega) \times R_{r-1}(\Omega) \times R_{r-1}(\Omega) \cap L_0^2(\Omega) \quad (34)$$

and its equal-order analogue

$$\overline{X}_h^{(r)} = \mathbf{V}_r(\Omega) \times R_r(\Omega) \times R_r(\Omega) \cap L_0^2(\Omega), \quad (35)$$

respectively, where $r > 1$ if $\|\cdot\|_{(h)}$ is the weighted L^2 norm, and $r \geq 1$ if $\|\cdot\|_{(h)}$ is the discrete negative norm.

A straightforward dimensional analysis shows that for the solenoidal vector fields in (12) and standard nodal functions $\psi_h \in [R_r](\Omega)$ we have

$$\int_{\varepsilon} [\mathbf{u}_h]^2 dl = O(h) \quad \text{and} \quad \int_{\varepsilon} [\nabla \times \psi_h]^2 dl = O(h^{-1}), \quad (36)$$

for some edge $\varepsilon \in \mathcal{E}_h$. Therefore, in order to preserve the relative scaling of the terms in the dS-VP functional (25) when using the piecewise solenoidal space (12) it is necessary to change the weight of the velocity jump term from h^{-1} to h^{-3} . Taking this and the divergence-free property of the velocity basis into consideration, we introduce a new functional

$$\begin{aligned} \widehat{J}_{(h)}^{V,\alpha}(\mathbf{u}_h, \omega_h, p_h; \mathbf{f}_h) &= \\ &\|\nabla \times \omega_h + \nabla p_h - \mathbf{f}_h\|_{(h)}^2 + \sum_{\kappa \in \mathcal{K}_h(\Omega)} \|\nabla \times \mathbf{u}_h - \omega_h\|_{0,\kappa}^2 + \sum_{\varepsilon \in \mathcal{E}_{h,0}} h^{-\alpha} \|[\mathbf{u}_h]\|_{0,\varepsilon}^2 \end{aligned} \quad (37)$$

and (33) becomes

$$\widehat{J}_{(h)}^V(\mathbf{u}_h, \omega_h, p_h; \mathbf{f}_h) := \widehat{J}_{(h)}^{V,-3}(\mathbf{u}_h, \omega_h, p_h; \mathbf{f}_h) \quad (38)$$

To demonstrate the role of proper weighting of the velocity jump we solve the two test problems using three different weights for this term in (37). Our implementation uses the equal order space (35) with $r = 2$. We set $\|\cdot\|_{(h)} = h\|\cdot\|_0$ and choose $\alpha = -1, -2, -3$. The C^0 least-squares solution of (21), implemented with the equal order space $X_h^{(2)}$, provides the benchmark. Figure 5 demonstrates that proper weighting of this term significantly reduces the mass loss in the least-squares solution. Yet, it also shows that if the changes in the scaling of the least-squares terms induced by the piecewise solenoidal velocity space (12) are not taken into consideration, conservation of mass suffers. Specifically, if the weight of the velocity jump is left at h^{-1} , as in the

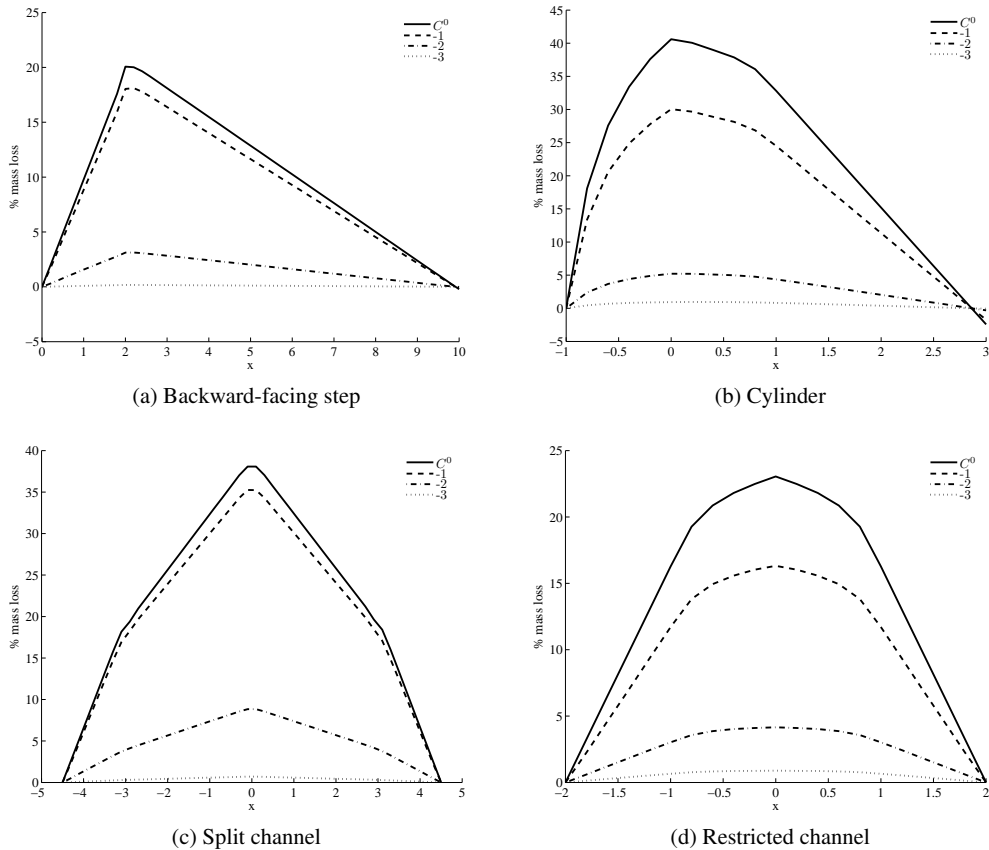


Figure 5. Comparison of the mass loss in the discontinuous velocity LSFEM (37) with $\|\cdot\|_{(h)} = h\|\cdot\|_0$, and $\alpha = -1, -2, -3$ vs. standard C^0 LSFEM (19).

dS-VP functional (25), then the peak mass loss in all four test problems is similar to the C^0 solution.

Figure 5 demonstrates that when using the correct weight on the jump term, (37) performs very well — i.e., the maximum mass loss in each test problem is less than 1% at 0.17%, 0.95%, 0.70%, and 0.88% for each test problem, respectively. However, we remark that the meshes used in the test cases are very well refined. On less refined meshes the mass loss for (37) is more evident. For example, the plots of mass loss in Figure 6 demonstrate that on a less refined mesh ($h \approx 0.07$), the maximum mass loss is around 2% even with the jump weight set at h^{-3} despite the piecewise solenoidal basis for the velocity field. When compared with the dS-VP formulation (25), the method exhibits considerably more mass loss. Because the exact velocity is divergence free, there is a scalar stream function ψ such that $\mathbf{u} = \nabla \times \psi$. The piecewise solenoidal velocity space $\mathbf{V}_r(\Omega)$ has this property locally — i.e., if $\mathbf{v}_h \in \mathbf{V}_r(\Omega)$. Thus, on every element $\kappa \in \mathcal{K}_h$, there is an implicit stream function ψ_κ such that $\mathbf{v}_h|_\kappa = \nabla \times \psi_\kappa$. Yet, the existence of an implicit stream function ψ_κ on each element does not imply that a piecewise solenoidal field $\mathbf{v}_h \in \mathbf{V}_r(\Omega)$ approximates the curl of a *global* stream function. This requires the implicit stream functions ψ_κ on adjacent elements to be nearly equal along the interfaces between the elements, and motivates the construction of a such a function.

3.1. Implicit Stream Function

Since we related $\mathbf{u} = \nabla \times \psi$, the jump in velocity in (38) only controls the continuity of $\nabla \times \psi_k$, and does not directly “glue” ψ_k across element interfaces. To enforce this on the implicit stream

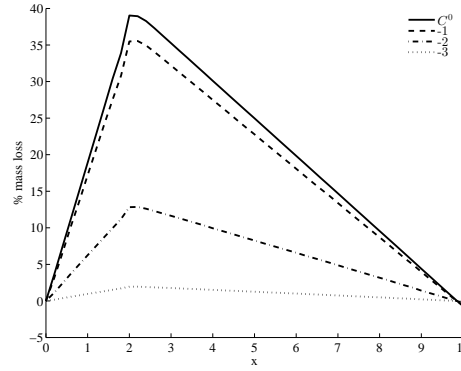


Figure 6. Comparison of the mass loss in the discontinuous velocity LSFEM (37) with $\|\cdot\|_{(h)} = h\|\cdot\|_0$, and $\alpha = -1, -2, -3$ vs. a standard C^0 LSFEM (19) for the backward step domain on a less refined mesh (1649 triangles).

functions, we propose to augment (38) with terms that imitate the jumps of the discontinuous stream function in (25).

For simplicity, we express the main idea using the trapezoidal rule to approximate the line integrals in these jumps. Let $V_0 = V_0(\varepsilon)$ and $V_1 = V_1(\varepsilon)$ be the endpoints of edge $\varepsilon \in \mathcal{E}_h$. Then,

$$\int_{\varepsilon} [\psi_h]^2 d\ell \approx \frac{|\varepsilon|}{2} \left([\psi_h(V_0)]^2 + [\psi_h(V_1)]^2 \right). \quad (39)$$

Implementation of this formula requires reconstruction of the implicit stream function values at V_0 and V_1 using the piecewise solenoidal velocity field. To this end we denote the two elements that share an edge $\varepsilon = (\varepsilon_1, \varepsilon_2)$ by $\kappa^+(\varepsilon)$ and $\kappa^-(\varepsilon)$. For a given $\mathbf{u}_h \in \mathbf{V}_r(\Omega)$ let ψ_k^+ and ψ_k^- denote its implicit stream functions on each $\kappa^+(\varepsilon)$ and $\kappa^-(\varepsilon)$, respectively:

$$\mathbf{u}_h^{\pm} = (u_{h,1}^{\pm}, u_{h,2}^{\pm}) = \mathbf{u}_h|_{\kappa^{\pm}(\varepsilon)} = (\partial_y \psi_k^{\pm}, -\partial_x \psi_k^{\pm}). \quad (40)$$

Solving for the gradients of the implicit stream functions yields

$$\nabla \psi_k^{\pm} = (-u_{h,2}^{\pm}, u_{h,1}^{\pm}). \quad (41)$$

As a result, along edge ε

$$\frac{d\psi_k^{\pm}}{ds}|_{\varepsilon} = \nabla \psi_k^{\pm} \cdot \varepsilon = (u_{h,1}^{\pm} \varepsilon_2 - u_{h,2}^{\pm} \varepsilon_1) = \mathbf{u}_h^{\pm} \times \varepsilon. \quad (42)$$

The values of the implicit stream functions ψ_k^{\pm} at V_0 and V_1 can be determined by solving the edge ODEs

$$\begin{cases} \frac{d\psi_k^{\pm}}{ds}|_{\varepsilon} = (\mathbf{u}_h^{\pm} \times \varepsilon)|_{\varepsilon} & \text{and} & \begin{cases} \frac{d\psi_k^{\pm}}{ds}|_{\varepsilon} = -(\mathbf{u}_h^{\pm} \times \varepsilon)|_{\varepsilon} \\ \psi_k^{\pm}(|\varepsilon|) = C_1 \end{cases} \end{cases} \quad (43)$$

for $0 < s < |\varepsilon|$. If the mesh is aligned with the coordinate axes, then closed form solutions are straightforward, while for general unstructured grids we solve (43) numerically. For illustration, using the explicit Euler method yields

$$\begin{aligned} \psi_k^{\pm}(V_0) &= \psi_k^{\pm}(0) \approx C_1 - |\varepsilon|(\mathbf{u}_h^{\pm}(V_0) \times \varepsilon) \\ \psi_k^{\pm}(V_1) &= \psi_k^{\pm}(|\varepsilon|) \approx C_0 + |\varepsilon|(\mathbf{u}_h^{\pm}(V_1) \times \varepsilon). \end{aligned} \quad (44)$$

Then, using (44) in (39) gives the approximation

$$\int_{\varepsilon} [\psi_h]^2 d\ell \approx \frac{|\varepsilon|^3}{2} \left([(\mathbf{u}_h(V_0) \times \varepsilon)]^2 + [(\mathbf{u}_h(V_1) \times \varepsilon)]^2 \right). \quad (45)$$

Recall that in the dS-VP functional (25) we weight the integral of $[\psi_h]^2$ along ε by h^{-3} . To determine the proper weight for the approximation (45), observe that dimensional analysis of the terms yields

$$\frac{|\varepsilon|^3}{2} [(\mathbf{u}_h(V_0) \times \varepsilon)]^2 + \left([(\mathbf{u}_h(V_1) \times \varepsilon)]^2 \right) = O(h^3) \quad \text{and} \quad \int_e [\psi_h]^2 dl = O(h). \quad (46)$$

Therefore, to preserve the relative scaling of the terms in the dS-VP functional (25) when the stream function jump is approximated by (45) it is necessary to change the weight of this term from h^{-3} to h^{-5} . We add the properly weighted term (45) to (38) to arrive at the final form of the discontinuous velocity, vorticity, pressure (dV-VP) least-squares functional:

$$\begin{aligned} \tilde{J}_{(h)}^V(\mathbf{u}_h, \omega_h, p_h; \mathbf{f}_h) &= \|\nabla \times \omega_h + \nabla p_h - \mathbf{f}_h\|_{(h)}^2 + \sum_{k \in K(\Omega)} \|\nabla \times \mathbf{u}_h - \omega_h\|_{0,k}^2 \\ &+ \sum_{e \in E(\hat{\Omega})} h^{-3} \|\mathbf{u}_h\|_{0,e}^2 + h^{-5} \frac{|\varepsilon|^3}{2} \left([(\mathbf{u}_h(V_0) \times \varepsilon)]^2 + [(\mathbf{u}_h(V_1) \times \varepsilon)]^2 \right). \end{aligned} \quad (47)$$

To evaluate the role of (45) we solve the test problems using both (38) and (47), implemented with the equal-order space (35), and $r = 2$. Figure 7 shows that inclusion of (45) reduces the mass loss from 0.17%, 0.95%, 0.70%, and 0.88% to 0.04%, 0.27%, 0.18%, and 0.13% for each of the test problems respectively. When compared with (38), this is a reduction in mass loss of about 25% for each test problem. The improvement in the mass conservation due to (45) is even more impressive on coarser grids where it can reach 50%.

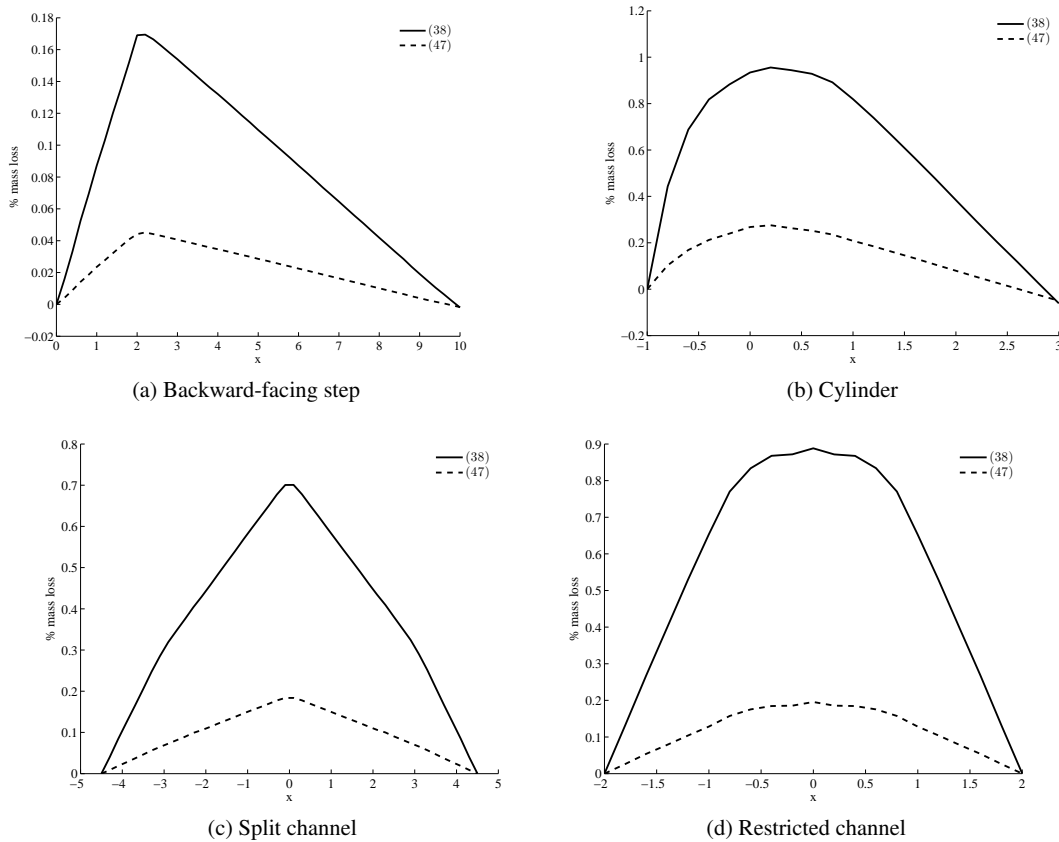


Figure 7. Comparison of the mass loss in the discontinuous velocity LSFEM with $\|\cdot\|_{(h)} = h\|\cdot\|_0$, with (47) vs. without (38) the implicit stream function term.

Remark 3

While the piecewise solenoidal fields $\mathbf{u}_h \in \mathbf{V}_r(\Omega)$ are curls of discontinuous implicit stream functions $\psi \in [R]_{r+1}(\Omega)$, the new dV-VP least-squares method is not equivalent to the dS-VP formulation (25), and has some important computational advantages. Because the velocity is approximated directly, implementation of the velocity boundary condition is straightforward for (47). Furthermore, for moderate polynomial degrees the dimension of $[R]_{r+1}(\Omega)$ is almost twice that of the piecewise solenoidal space $\mathbf{V}_r(\Omega)$.

3.2. Preconditioning of the algebraic equations

We denote \mathbb{K} as the symmetric and positive definite matrix resulting from the dV-VP least-squares functional (47). For a test function $(\mathbf{u}_i, \omega_i, p_i) \in \overline{X}_h^r$, or $(\mathbf{u}_i, \omega_i, p_i) \in \overline{X}_h^{(r)}$ we see that the weak form of (47) leads to the following 3×3 system for \mathbb{K} :

$$\begin{pmatrix} \mathbb{K}_{\mathbf{u},\mathbf{u}} & \mathbb{K}_{\mathbf{u},\omega} & \mathbf{0} \\ \mathbb{K}_{\mathbf{u},\omega} & \mathbb{K}_{\omega,\omega} & \mathbb{K}_{\omega,p} \\ \mathbf{0} & \mathbb{K}_{\omega,p} & \mathbb{K}_{p,p} \end{pmatrix} \begin{pmatrix} \vec{u} \\ \vec{\omega} \\ \vec{p} \end{pmatrix} = \begin{pmatrix} f_{\mathbf{u}} \\ f_{\omega} \\ f_p \end{pmatrix} \quad (48)$$

where

$$\begin{aligned} (\mathbb{K}_{\mathbf{u},\mathbf{u}})_{ij} &= \sum_k (\nabla \times \mathbf{u}_i, \nabla \times \mathbf{u}_j)_{0,k} + \sum_{\varepsilon} h^{-3} ([\mathbf{u}_i], [\mathbf{u}_j])_{0,\varepsilon} \\ &+ \sum_{\varepsilon} h^{-5} \frac{|\varepsilon|^3}{2} \left([(\mathbf{u}_i(V_1) \times \varepsilon)][(\mathbf{u}_j(V_1) \times \varepsilon)] + [(\mathbf{u}_i(V_0) \times \varepsilon)][(\mathbf{u}_j(V_0) \times \varepsilon)] \right), \end{aligned} \quad (49)$$

and

$$(\mathbb{K}_{\mathbf{u},\omega})_{ij} = (\nabla \times \mathbf{u}_i, \omega_j), \quad (50a)$$

$$(\mathbb{K}_{\omega,\omega})_{ij} = h^2 (\nabla \times \omega_i, \nabla \times \omega_j), \quad (50b)$$

$$(\mathbb{K}_{\omega,p})_{ij} = h^2 (\nabla \times \omega_i, \nabla p_j) = h^2 (\mathbf{n} \times \omega, \nabla p)_{0,\Gamma}, \quad (50c)$$

$$(\mathbb{K}_{p,p})_{ij} = h^2 (\nabla p_i, \nabla p_j). \quad (50d)$$

The h^2 weights arise from the use of the mesh-dependent norm $\|\cdot\|_{(h)} = h \|\cdot\|_0$. Dimensional analysis of the blocks in \mathbb{K} suggests the approximation

$$\mathbb{K} \sim \tilde{\mathbb{K}} = \begin{pmatrix} h^{-2} \mathbb{M}_{\mathbf{u},\mathbf{u}} & h \mathbb{D}_{\mathbf{u},\omega} & \mathbf{0} \\ h \mathbb{D}_{\mathbf{u},\omega}^T & h^2 \mathbb{M}_{\omega,\omega} & h^2 \mathbb{M}_{\Gamma} \\ \mathbf{0} & h^2 \mathbb{M}_{\Gamma}^T & h^2 \mathbb{M}_{p,p} \end{pmatrix}, \quad (51)$$

where $\mathbb{M}_{\mathbf{u},\mathbf{u}}$, $\mathbb{M}_{\omega,\omega}$, and $\mathbb{M}_{p,p}$ are unscaled mass matrices, \mathbb{M}_{Γ} is the unscaled ‘‘boundary’’ mass matrix acting only on boundary degrees of freedom, and $\mathbb{D}_{\mathbf{u},\omega}$ is unscaled ‘‘difference’’ matrix. The structure of $\tilde{\mathbb{K}}$ indicates that reduction of its condition number may be possible by balancing the equations through the diagonal preconditioner

$$\mathbb{D}_p = \begin{pmatrix} h^p \mathbb{I} & \mathbf{0} & \mathbf{0} \\ \mathbf{0} & \mathbb{I} & \mathbf{0} \\ \mathbf{0} & \mathbf{0} & \mathbb{I} \end{pmatrix}, \quad (52)$$

where p is a suitable parameter. Figure 8 shows numerical estimate of the condition number of $\mathbb{D}_p^{1/2} \tilde{\mathbb{K}} \mathbb{D}_p^{1/2}$ as function of p . The smallest condition number is achieved when $p = 3$. Our computational studies confirm that this value also extends to \mathbb{K} , and thus the preconditioned system becomes

$$\mathbb{K}_{prec} = \mathbb{D}_3^{1/2} \mathbb{K} \mathbb{D}_3^{1/2}. \quad (53)$$

Remark 4

A similar diagonal preconditioner can be used for the dS-VP formulation (25) and in this case, we observed similar improvements in condition number.

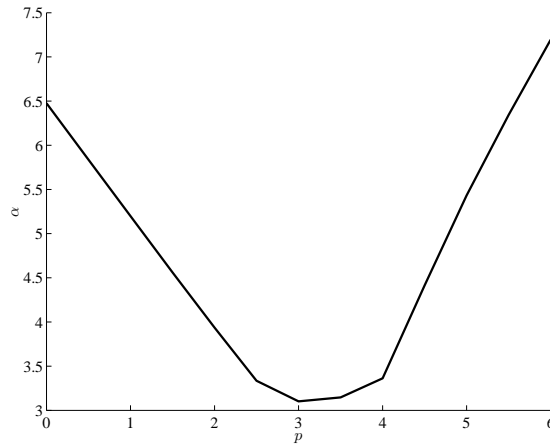


Figure 8. Growth in condition number $O(h^{-\alpha})$ of the preconditioned approximate matrix $\mathbb{D}_p^{1/2} \tilde{\mathbb{K}} \mathbb{D}_p^{1/2}$ as function of p .

4. COMPUTATIONAL STUDY

In this section we study the computational properties of the proposed dV-VP least-squares method presented in the previous sections. We implement the method using the equal-order space (35) with $r = 2$. Specifically, we study numerically, the convergence rates for the method and the effectiveness of the proposed preconditioner. In addition, velocity profiles for each test problem are plotted for the C^0 formulation (6) and the dV-VP formulation (47) thus visually demonstrating the improvement in mass conservation.

4.1. Convergence

In this section we compare convergence rates of the dV-VP LSFEM with and without the integral jump term. The computational domain Ω is the unit square. \mathcal{K}_h is uniform partition of Ω into square elements with side length equal to $h_i = 2^{-i}$ for $i = 1, 2, 3, 4, 5$. The convergence rates are estimated using a manufactured solution, where the exact solution is selected as

$$\mathbf{u} = \begin{bmatrix} -\pi \sin(\pi y) \\ \pi \sin(\pi x) \end{bmatrix}, \quad \omega = \nabla \times \mathbf{u} = \pi^2 (\cos(\pi x) + \cos(\pi y)), \quad p = \sin(x) \exp(y),$$

and hence, the corresponding right hand side is

$$\mathbf{f} = \begin{bmatrix} -\pi^3 \sin(\pi y) + \cos(x) \exp(y) \\ \pi^3 \sin(\pi x) + \sin(x) \exp(y) \end{bmatrix}.$$

LSFEM	$\hat{J}_{(h)}^V$ (38)				$\tilde{J}_{(h)}^V$ (47)				
	h	$\ \mathbf{u} - \mathbf{u}_h\ _0$	rate	$\ \mathbf{u} - \mathbf{u}_h\ _1$	rate	$\ \mathbf{u} - \mathbf{u}_h\ _0$	rate	$\ \mathbf{u} - \mathbf{u}_h\ _1$	rate
	1/4	8.118e-3	–	2.274e-1	–	8.116e-3	–	2.274e-1	–
	1/8	1.071e-3	2.922	5.680e-2	2.001	1.071e-3	2.922	5.680e-2	2.001
	1/16	1.366e-4	2.947	1.419e-2	2.001	1.366e-4	2.946	1.419e-2	2.001
	1/32	1.769e-5	2.950	3.547e-3	2.001	1.769e-5	2.950	3.547e-3	2.001

Table I. Convergence rates of velocity \mathbf{u} , for (38) and (47).

LSFEM	$\widehat{J}_{(h)}^V$ (38)				$\widetilde{J}_{(h)}^V$ (47)				
	h	$\ \omega - \omega_h\ _0$	rate	$\ \omega - \omega_h\ _1$	rate	$\ \omega - \omega_h\ _0$	rate	$\ \omega - \omega_h\ _1$	rate
1/4	5.040e-2	–	1.007e0	–	5.026e-2	–	1.006e0	–	–
1/8	4.562e-3	3.466	2.147e-1	2.230	4.563e-3	3.461	2.147e-1	2.228	–
1/16	5.874e-4	3.211	5.784e-2	2.061	5.876e-4	3.209	5.785e-2	2.061	–
1/32	1.016e-4	2.982	1.908e-2	1.906	1.016e-4	2.981	1.908e-2	1.905	–

Table II. Convergence rates of vorticity ω , for (38) and (47).

LSFEM	$\widehat{J}_{(h)}^V$ (38)				$\widetilde{J}_{(h)}^V$ (47)				
	h	$\ p - p_h\ _0$	rate	$\ p - p_h\ _1$	rate	$\ p - p_h\ _0$	rate	$\ p - p_h\ _1$	rate
1/4	8.320e-2	–	7.349e-1	–	8.292e-2	–	7.331e-1	–	–
1/8	6.525e-3	3.673	1.088e-1	2.756	6.542e-3	3.664	1.089e-1	2.751	–
1/16	9.049e-4	3.261	2.325e-2	2.491	9.086e-4	3.256	2.327e-2	2.489	–
1/32	1.922e-4	2.912	5.603e-3	2.333	1.927e-4	2.910	5.609e-3	2.333	–

Table III. Convergence rates of pressure p , for (38) and (47).

Tables I-III demonstrate that the method indeed exhibits the optimal convergence rates as expected from Theorem 1. However, since we the vorticity and pressures are implemented using quadratic basis functions, we observe that

$$\|\omega - \omega^h\|_0 = \|p - p^h\|_0 = O(h^3) \quad \text{and} \quad \|\omega - \omega^h\|_1 = \|p - p^h\|_1 = O(h^2) \quad (54)$$

which is expected for quadratic basis functions. Furthermore, it can be seen that the inclusion of the jump term enforcing the continuity of the implicit stream function, which improved the mass conservation as demonstrated in Section 3, does not affect the convergence rates of the method.

4.2. Conservation of mass

In Figures 9, 10, 11, and 12 the velocity field is plotted for (19) and (47) with colors representing the magnitude of the vector field. For the backward step, Figure 9 shows that the magnitude of the velocity field in the C^0 formulation decreases as the flow reaches the re-entrant corner at $x = 2$ while for (47), the initial velocity profile is propagated until the re-entrant corner. For the second test problem, the difference in intensities of the velocity profile at $x = 0$ is clear with a maximum velocity of almost 10.0 in (47) compared to only 5.0 for (19). In the split channel domain, an initial channel of height 1.0 is split into two channels of height 0.5. Although the height of the two split channels are 0.5, the diameter of the opening is less due to the angle of the split. The velocity profile for (47) demonstrates an increase in velocity in the channels with the velocity profile being propagated through the channels. In the C^0 solution, the magnitude of the velocity does not increase relative to the initial velocity and additionally, the magnitude of the velocity dissipates within each of the split channels. The behavior in the restricted channel domain is similar to that of the cylinder flow problem with (47) pushing twice as much flow as (19) at the narrowest part of the opening.

4.3. Preconditioning

We next study the effectiveness of the preconditioner in (53). We estimate numerically the growth in condition number of the matrix as the mesh is refined for formulations before and after the application of the preconditioners.

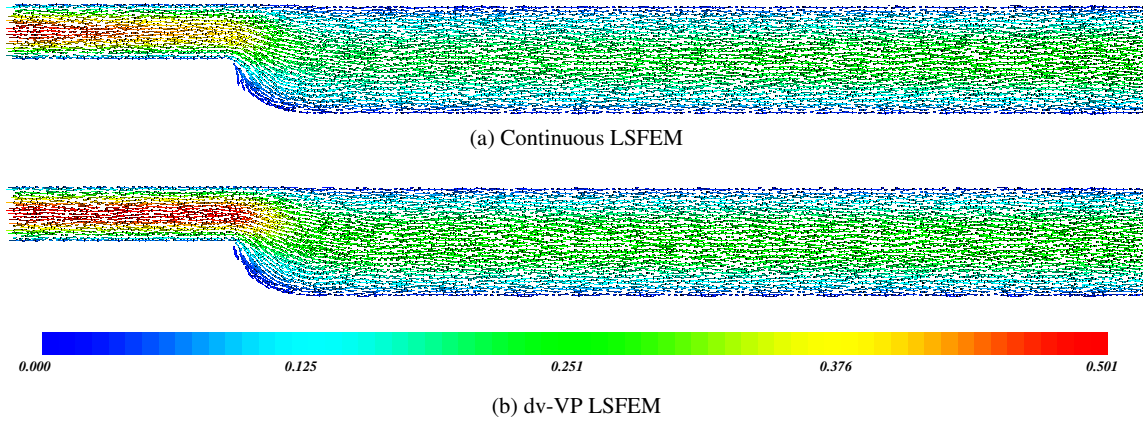


Figure 9. Velocity plot of (6) and (47) on the backward step domain, Test Problem 1.

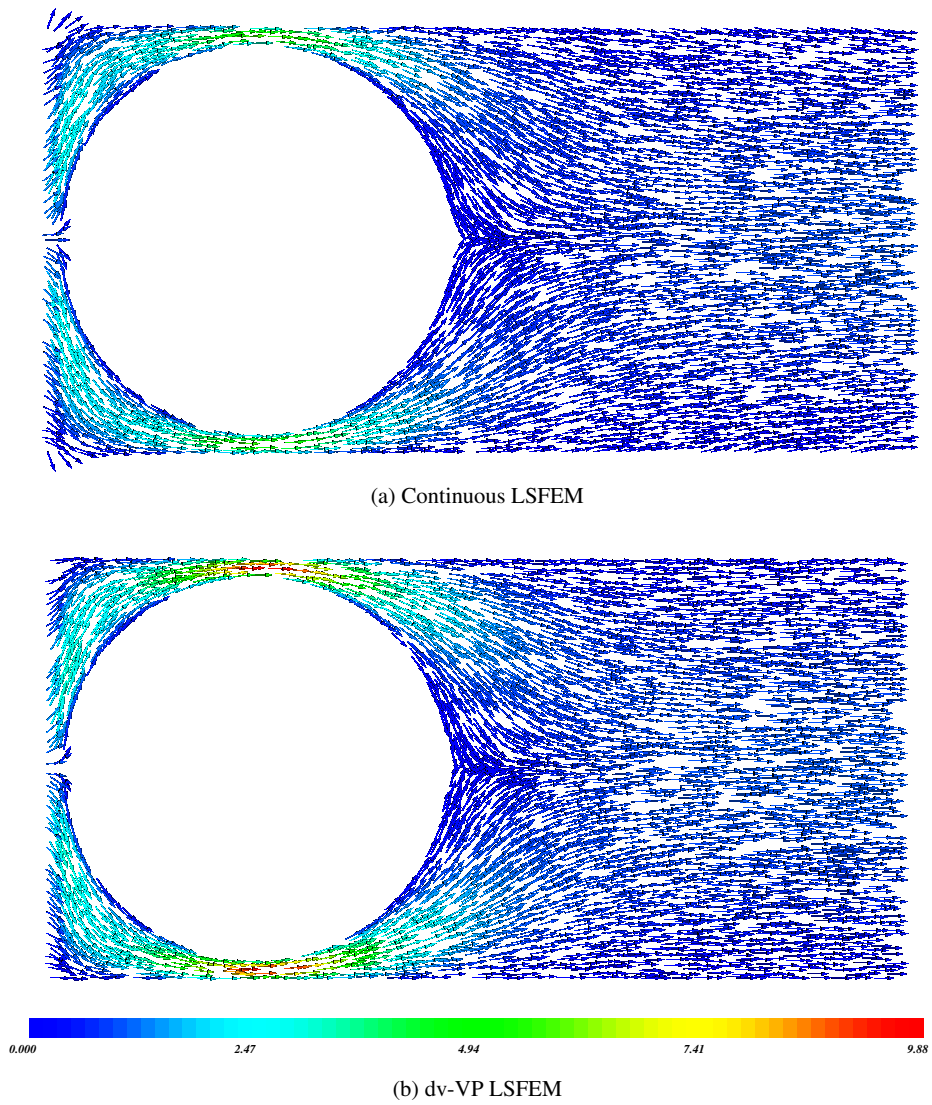


Figure 10. Velocity plot of (6) and (47) on the cylinder flow domain, Test Problem 2.

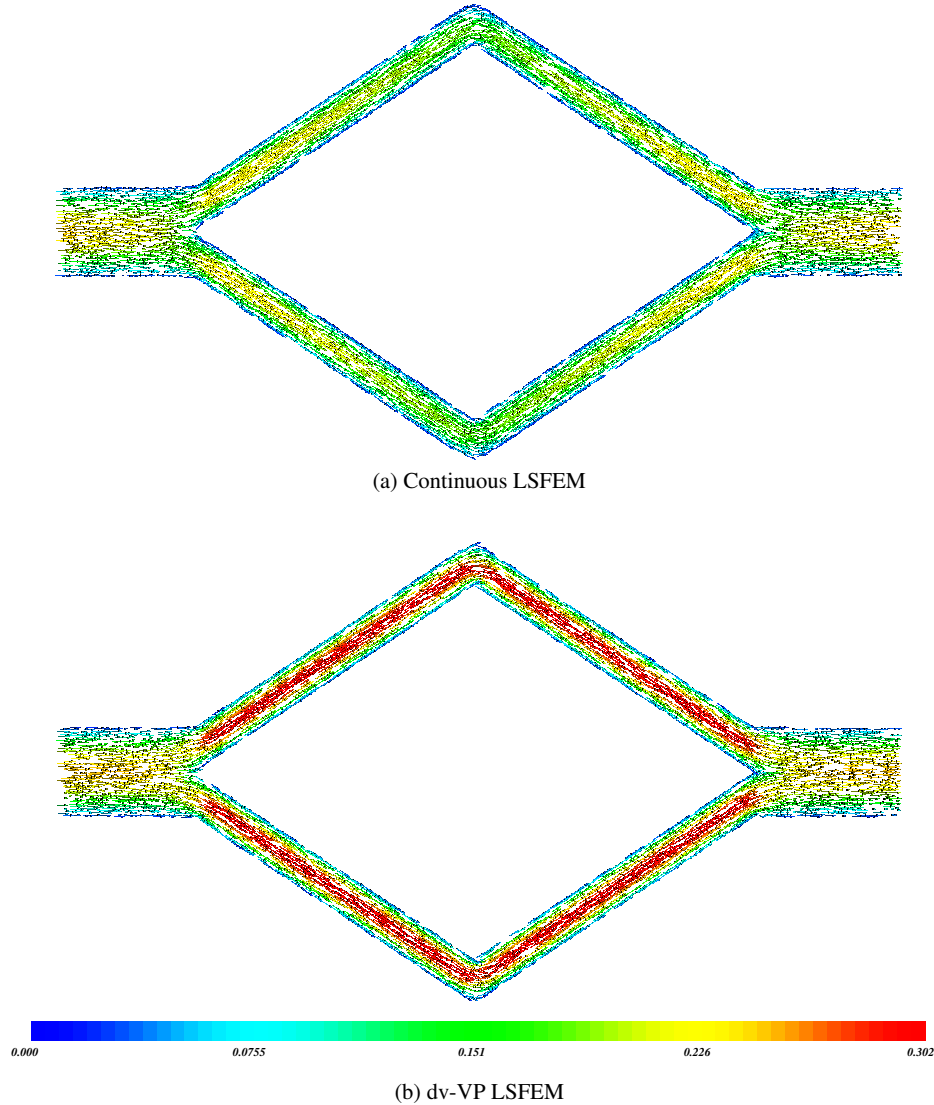


Figure 11. Velocity plot of (6) and (47) on the split channel domain, Test Problem 3.

Table IV demonstrates that without a preconditioner, the growth in condition number of (47) as the mesh is refined is approximately $O(h^{-6})$. As a point of reference, the dependence on h is $O(h^{-4})$ and $O(h^{-2})$ for (19) and (20) respectively; see [4, Theorem 4.8, p.119] and [4, Theorem 4.10, p.126]. The preconditioner (53) reduces the growth in condition number close to that of the discrete negative norm.

5. CONCLUSIONS

In this paper, we continue the efforts of [6] to improve mass conservation in least-squares finite elements for the Stokes equations, while preserving the most attractive properties of this class of methods. To this end, we use a nonconforming piecewise divergence-free basis for the velocity field. To this end, we use a nonconforming piecewise divergence-free basis for the velocity field. However, numerical experiments illustrate that although introduction of a divergence-free basis for the velocity improved mass conservation, it alone is insufficient to reduce mass loss to levels

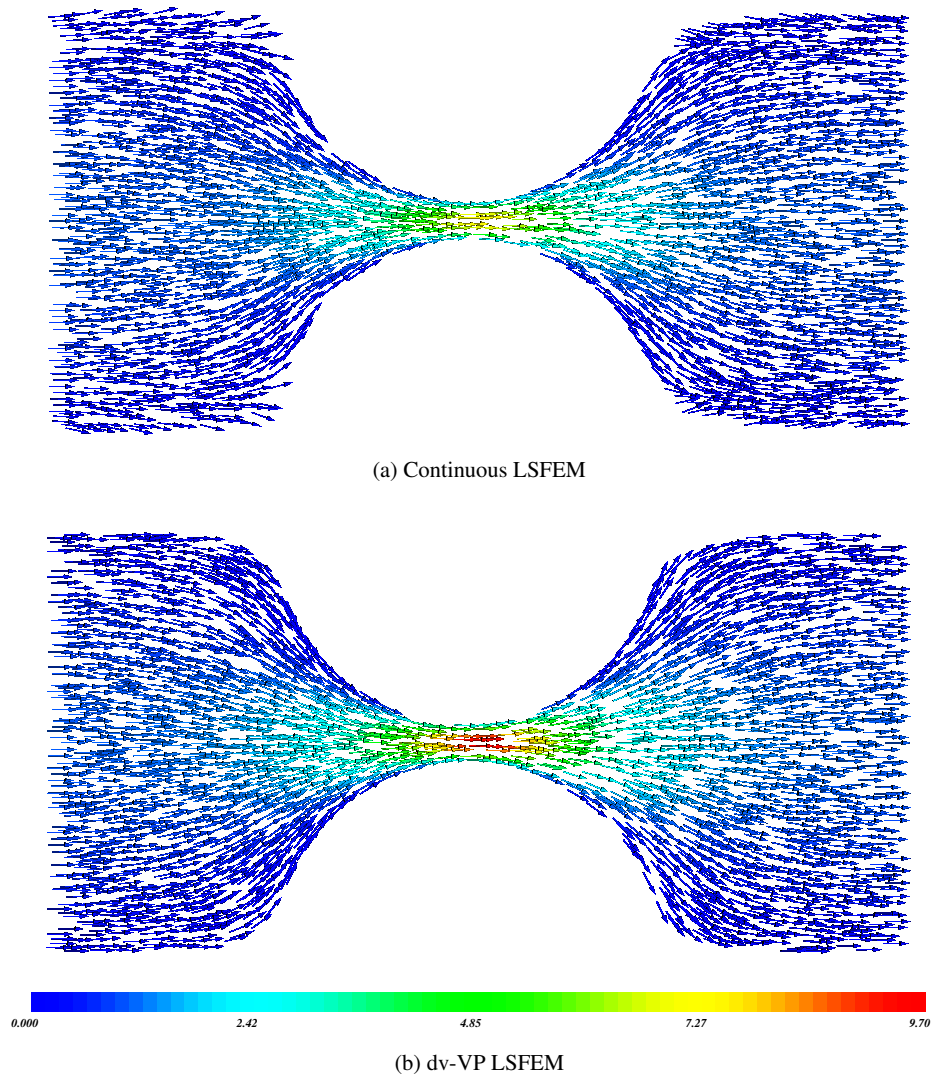


Figure 12. Velocity plot of (6) and (47) on the restricted channel domain, Test Problem 4.

LSFEM	no preconditioning	with preconditioning
$J_{(h)}^V$	3.9	3.9
$\hat{J}_{(h)}^V$	5.8	2.9
$\tilde{J}_{(h)}^V$	5.8	2.8

Table IV. Growth in condition number $O(h^{-\alpha})$ for original and preconditioned matrices for (33), (38), and (47).

comparable to the dS-VP formulation of [6]. The mass conservation is further improved by enforcing global continuity of an implicit stream function. Finally, a simple diagonal preconditioner is introduced to reduce the growth in condition number relative to mesh refinement down to levels comparable to Galerkin and discrete negative norm methods.

REFERENCES

1. G. A. BAKER, W. N. JUREIDINI, AND O. A. KARAKASHIAN, *Piecewise solenoidal vector fields and the stokes problem*, SIAM Journal on Numerical Analysis, 27 (1990), pp. 1466–1485.
2. P. BOCHEV, *Negative norm least-squares methods for the velocity-vorticity-pressure Navier-Stokes equations*, Numer. Meth. PDEs, 15 (1999), pp. 237–256.
3. P. BOCHEV AND M. GUNZBURGER, *Analysis of least-squares finite element methods for the Stokes equations*, Math. Comp., 63 (1994), pp. 479–506.
4. ———, *Least-Squares finite element methods*, vol. 166 of Applied Mathematical Sciences, Springer Verlag, 2009.
5. ———, *A locally conservative mimetic least-squares finite element method for the Stokes equations*, in Proceedings of LSSC 2009, I. Lirkov, S. Margenov, and J. Wasniewski, eds., vol. 5910 of Springer Lecture Notes in Computer Science, 2009, pp. 637–644.
6. P. BOCHEV, J. LAI, AND L. OLSON, *A locally conservative, discontinuous least-squares finite element method for the stokes equations*, International Journal for Numerical Methods in Fluids, (2011).
7. P. BOCHEV, D. RIDZAL, AND K. PETERSON, *Intrepid: Interoperable Tools For Compatible Discretizations*. <http://trilinos.sandia.gov/packages/intrepid/>, 2010.
8. P. BOLTON AND R. W. THATCHER, *On mass conservation in least-squares methods*, J. Comput. Phys., 203 (2005), pp. 287–304.
9. J. H. BRAMBLE AND J. E. PASCIAK, *Least-squares methods for stokes equations based on a discrete minus one inner product*, Journal of Computational and Applied Mathematics, 74 (1996), pp. 155 – 173.
10. C. L. CHANG AND J. J. NELSON, *Least-squares finite element method for the stokes problem with zero residual of mass conservation*, SIAM Journal on Numerical Analysis, 34 (1997), pp. pp. 480–489.
11. ———, *Least-squares finite element method for the Stokes problem with zero residual of mass conservation*, SIAM J. Numer. Anal., 34 (1997), pp. 480–489.
12. P. CIARLET, *The Finite Element Method for Elliptic Problems*, SIAM Classics in Applied Mathematics, SIAM, Philadelphia, 2002.
13. B. COCKBURN, F. LI, AND C.-W. SHU, *Locally divergence-free discontinuous galerkin methods for the maxwell equations*, Journal of Computational Physics, 194 (2004), pp. 588 – 610.
14. A. ERN AND J.-L. GUERMOND, *Theory and Practice of Finite Elements*, no. 159 in Applied Mathematical Sciences, Springer Verlag, New York, 2004.
15. M. W. GEE, C. M. SIEFERT, J. J. HU, R. S. TUMINARO, AND M. G. SALA, *ML 5.0 Smoothed Aggregation User's Guide*, Tech. Rep. SAND2006-2649, Sandia National Laboratories, Albuquerque, NM, 2006.
16. M. D. GUNZBURGER, *Finite Element Methods for Viscous Incompressible Flows*, Academic, Boston, 1989.
17. M. A. HEROUX, R. A. BARTLETT, V. E. HOWLE, R. J. HOEKSTRA, J. J. HU, T. G. KOLDA, R. B. LEHOUCQ, K. R. LONG, R. P. PAWLOWSKI, E. T. PHIPPS, A. G. SALINGER, H. K. THORNQUIST, R. S. TUMINARO, J. M. WILLENBRING, A. WILLIAMS, AND K. S. STANLEY, *An overview of the Trilinos project*, ACM Trans. Math. Softw., 31 (2005), pp. 397–423.
18. J. J. HEYS, E. LEE, T. A. MANTEUFFEL, AND S. F. MCCORMICK, *An alternative least-squares formulation of the Navier-Stokes equations with improved mass conservation*, J. Comput. Phys., 226 (2007), pp. 994–1006.
19. J. J. HEYS, E. LEE, T. A. MANTEUFFEL, S. F. MCCORMICK, AND J. W. RUGE, *Enhanced mass conservation in least-squares methods for Navier-Stokes equations*, SIAM J. Sci. Comput., 31 (2009), pp. 2303–2321.
20. B.-N. JIANG AND C. CHANG, *Least-squares finite elements for the Stokes problem*, Comput. Meth. Appl. Mech. Eng., 78 (1990), pp. 297–311.
21. B.-N. JIANG AND V. SONNAD, *Least-squares solution of incompressible Navier-Stokes equations with the p-version of finite elements*, Tech. Rep. 91-14, NASA, Cleveland, 1991.
22. O. KARAKASHIAN AND T. KATSAOUNIS, *Numerical simulation of incompressible fluid flow using locally solenoidal elements*, Computers & Mathematics with Applications, 51 (2006), pp. 1551 – 1570.
23. M. CROUZEIX AND P. RAVIART, *Conforming and nonconforming finite element methods for solving the stationary Stokes equations*, RAIRO Model. Math. Anal. Numer., 3 (1973), pp. 33–76.
24. J. P. PONTAZA AND J. N. REDDY, *Spectral/hp least-squares finite element formulation for the navier-stokes equations*, Journal of Computational Physics, 190 (2003), pp. 523 – 549.
25. M. M. PROOT AND M. I. GERRITSMA, *Mass- and momentum conservation of the least-squares spectral element method for the stokes problem*, J. Sci. Comput., 27 (2006), pp. 389–401.